A COMPACT DOPPLER WIND LIDAR
FOR CONTROLLING THE OPERATION OF WIND TURBINES

Paul Gerke Hofmeister[1], Christoph Bollig[1,2], Sarah Fayed[1,3], Martin Kunze[1,4], and Rainer Reuter[1]

1. Carl von Ossietzky University of Oldenburg, Institute of Physics, Section Marine Physics, and ForWind Center for Wind Energy Research, D-26111 Oldenburg, Germany; {paul.gerke.hofmeister / rainer.reuter}(at)uni-oldenburg.de
2. now with: Abacus Laser, D-37120 Bovenden, Germany; info(at)abacus-laser.com
3. now with: University of Applied Sciences Emden/Leer, D-26723 Emden, Germany; sarah.fayed(at)hs-emden-leer.de
4. dipl.ing.martin.kunze(at)gmx.de

ABSTRACT

A robust and compact lidar for wind field detection has been developed for operation in the nacelle of wind turbines. The lidar measures wind speed along the line-of-sight of the laser beam with a 15 m range resolution along distances of 100 to 400 m depending on atmospheric aerosol content. An inclined orientation with respect to the rotor axis results in a conical scan of the incoming wind field, from which range-resolved data of the average wind velocity over the scanned cross-section are calculated. Application of the instrument aims at an improved turbine control by optimizing the pitch angle of rotor blades based on remotely sensed data, instead of reacting to wind field fluctuations which have already caused changes in rotational speed or loads. A predictive knowledge of wind conditions also allows for a precise evaluation of turbine power performance. The data are particularly useful for reducing high loads from gusts which otherwise cannot be detected in time.

In this paper, the conceptual layout of *Whirlwind 1* is described. Wind speed data are derived from the Doppler shift of backscattered laser radiation from aerosols which is interferometrically detected. Laser source is a diode laser pumped fibre amplifier seeded by a single-frequency diode laser emitting eye-safe radiation at 1.5 µm wavelength. The Doppler shifted laser frequency is detected with a Fast Fourier Transform of the signal return and converted to wind speeds in 37 range gates, each of 30 m length with a 50% overlap. The compact aluminium casing includes all components, i.e., the fibre laser, the signal detector, a Field Programmable Gate Array for fast data processing, a 3-axes accelerometer, and a compact industrial PC. First results of wind field measurements obtained with the prototype are presented.

INTRODUCTION

For multi-megawatt wind energy converters in large-scale wind farms, new and advanced control strategies are required. Dynamic wind loads have to be reduced efficiently and with minimal controller operation, in order to deliver electricity to the grid in an optimized way. Already small deviations from normal operation have to be detected using new instruments and adapted control strategies. Besides early detection of technical malfunctions of the turbines this includes the need of making available control strategies for optimization of power performance and reduction of loads based on predictive data on the inflowing wind field.

An instrument suitable for measuring wind using acoustical waves is the sodar (*so*und *d*etection *a*nd *r*anging). Installed on the ground and operated at near upward-looking directions, Sodar derives data on horizontal wind speeds from the Doppler shift Δf of signals returned to the instrument due to atmospheric inhomogeneities (1).

The advantage when compared with point measurements using cup anemometers on the nacelle of the turbine is the potential of sodar to measure wind in different atmospheric layers in the form of profiles by use of acoustic pulses and time-resolved signal detection.

An alternative to sodar is the lidar (*li*ght *d*etection *a*nd *r*anging) which remotely measures atmospheric parameters using laser radiation (2,3,4). With Doppler wind lidar, wind speed can be measured by analysing the Doppler shifted backscatter from aerosols that are assumed to propagate in the atmosphere at the same speed as the wind (5,6). The frequency f of radiation received by the lidar is Doppler shifted by Δf_D with respect to the laser frequency f_L,

$$f = f_L \pm \Delta f_D = f_L \left(1 \pm 2\frac{v}{c} \right) \qquad (1)$$

where v is the particle velocity component in the laser beam direction and c is the speed of light. The positive sign denotes the shift due to particles moving towards the lidar, and *vice versa* (please note: a slightly different equation holds with the acoustic Doppler effect). The factor 2 considers that Doppler shifts are caused by waves at the location of moving particles and secondly by the particles scattering radiation back to the lidar. With a near-infrared laser with 1.5 µm wavelength and assuming a wind speed of 1 m/s the Doppler shift becomes $\Delta f_D \approx 1.3$ MHz which is a very small deviation from the laser frequency $f_L = 200$ THz, making sophisticated methods necessary to be detected. The Doppler shift of a sodar emitting at 10 kHz is 60 Hz at 1 m/s wind speed.

As with sodar, profiles of wind speeds are obtained when using pulsed laser beams and measuring the time lapse of the received signal following the pulse emission. With the so-called continuous-wave Doppler lidar (7), profiles are obtained by focussing the laser beam and detection field-of-view to a specific distance which can be varied. Most of the received signal intensity originates from this focal volume which increases with increasing distance and limits the maximum range to less than approx. 200 m. By contrast, the geometric resolution of pulsed lidars remains nearly constant over the entire distance range (8). Pulsed lidars equipped with high power lasers have therefore been used for long range applications, e.g., for studying the wake of turbines and their impact on neighbouring turbines in wind farms over distances of several kilometres (9).

Ground-based wind lidars scanning the lower atmosphere at near-zenith angles are used to investigate wind in areas of wind farms on land and offshore (10,11). Sodar *versus* lidar comparisons in complex terrain showed consistent results giving evidence of their value for deriving predictive wind data for turbine control (12,13), but errors of 5-20% observed in another study indicate the need of further progress to improve and validate these methods (14).

Commercially available instruments are monostatic, i.e., the emitted beam axis and receiver axis coincide. Therefore, only the wind velocity component along the beam direction is obtained, and measuring wind vectors requires a scanning operation yielding data from which a wind vector representative for the investigated air volume can be estimated. Bistatic instruments produce an overlap of the emitter and receiver optical axes in a small air volume (15,16). However, controlling their optical alignment is difficult in a mechanically vibrating environment such as a turbine and would make highly stable mechanical scanners necessary.

Experimental lidars mounted on top of the nacelle of wind turbines were used for horizontal measurements to study wind conditions in the wake of turbines (17). Recently, it has been proposed to measure the inflowing wind field in front of the rotor with instruments mounted on the nacelle or in the spinner of wind energy converters. The rationale of this technically more demanding configuration results from numerical simulations: Range resolved data of the inflowing wind over distances of about two rotor diameters (2D) can be efficiently used for improving the control of wind turbines (18). Experimental configurations were tested successfully (19,20), but robust instruments for a long-time operational use in this harsh environment are not yet available.

In this paper, the concept of *Whirlwind 1,* a newly developed compact wind lidar for nacelle-based wind measurements is presented. The development aims at making available a robust instrument for increasing the power output of wind turbines through wind measurements ahead of the turbine and, more importantly, for reducing the risk of fatigue loads from gusts through predictive data of the wind field. The mechanical, optical and electronic characteristics and the methods of data processing are discussed. A focus of attention is the demand for an operational application as a com-

ponent of multi-MW turbines in offshore wind farms. Examples of wind data are presented which demonstrate the performance of the prototype instrument achieved so far.

METHODS

Requirements

The goal of lidar development is to make available an instrument for operational wind measurements as a future standard equipment of wind energy plants. The following performance shall be met:

> - A measuring range of 100 m or more with a 30 m distance resolution, depending of the turbine diameter
> - Representative evaluation of the wind velocity over the rotor cross section
> - Detection of gusts from lateral directions
> - Three-dimensional operation without use of a scanner that is subject to fatigue
> - A robust design which meets the requirements of a long-term operation with low maintenance in a vibrating environment across a wide range of temperatures and humidity.

Besides an improved regulation of the turbine operation, the predictive information on wind speeds shall enable us to reduce the load of pitch drives and to make use of more light- weight airfoil structures. Moreover, it enables a more detailed documentation of accidental damages.

The need of measuring representative wind vectors ahead of the rotor without using a mechanical scanner has led to the approach to integrate the lidar into the spinner of the turbine. An inclined optical axis of the lidar with respect to the spinner axis results in a conical scan while the rotor is turning. Compared with a setup mounted on top of the nacelle the instrument is better protected against weather, but the mechanical robustness must be higher due to rotation and vibrations in the spinner.
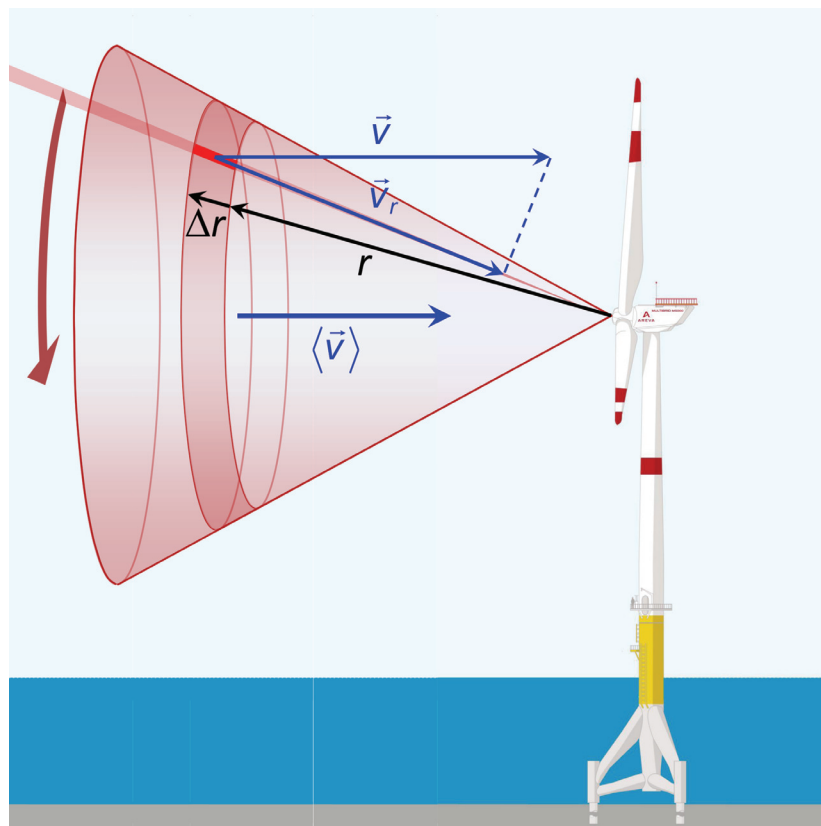

Figure 1: Simplified sketch of wind measured with a lidar installed in the spinner of a wind turbine. The wind velocity $\vec{v}$ in a sampling volume (bright red) is measured with its component $\vec{v}_r$ in the laser beam direction (red divergent line). The mean wind speed $\langle \vec{v} \rangle$ in a cross-section at distance r ahead is calculated by averaging the data obtained during a complete turn of the rotor.

With a lidar installed in the spinner wind data are obtained along profiles on the mantle of a cone which correspond to the wind speed in the laser beam direction (along the 'line-of-sight'), representative of air volumes defined by the local laser beam width and a length interval Δr, Figure 1. The range resolution Δr is set by the laser pulse length τ according to

$$\Delta r = c\tau/2 \qquad (2)$$

where c is the speed of light. The signal detection frequency bandwidth Δf should be sufficiently high to detect the temporal dynamics of the returned signal, i.e., $\Delta f \approx 1/\tau$.

Pixel distances along the circular cross-section of the cone depend on the laser pulse frequency and number of averaged single measurements, as well as on the rotational speed of the turbine. The profiles extend from a minimum distance up to a maximum range which is variable due to varying aerosol concentration. The minimum profiling distance is due to straylight from the laser emission which must decay before first valid data can be taken. From the data, average wind vectors are derived which are representative of the area of the conical scan at a given distance $(r, r + \Delta r)$.
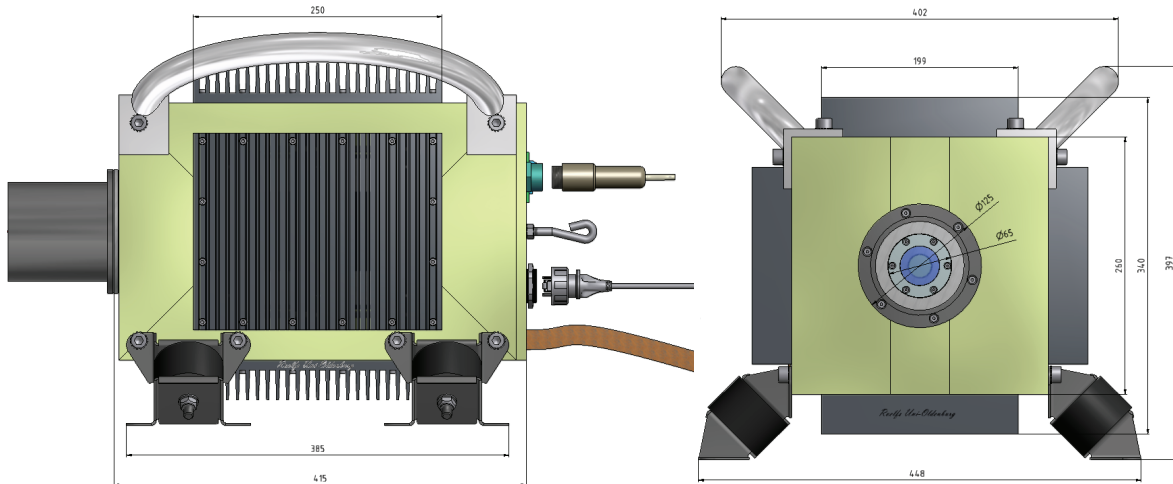

Figure 2: Layout of the lidar, side (left) and front (right) view. Dimensions are in millimetres.
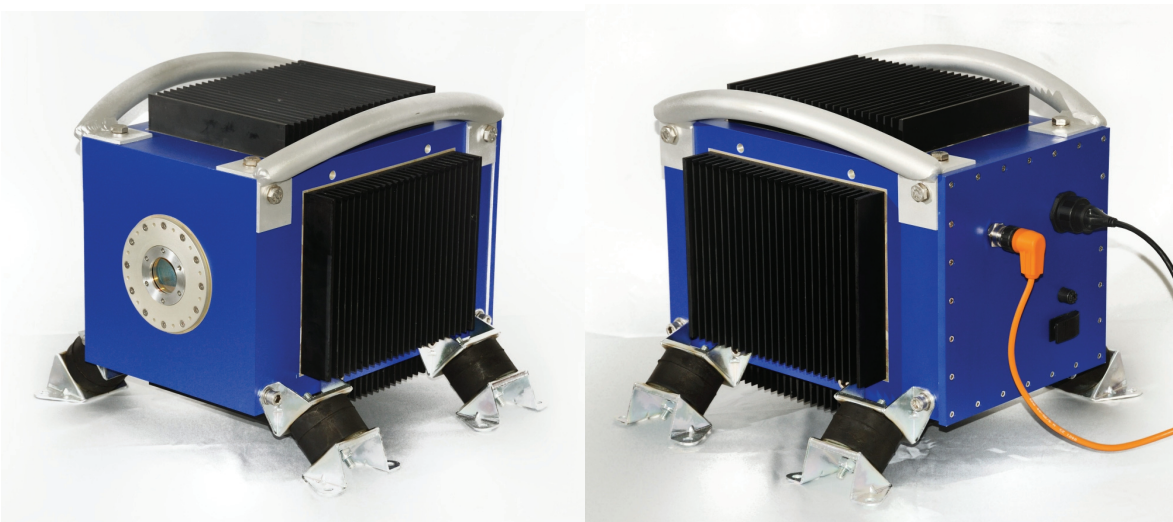

Figure 3: Front (left) and rear (right) view of the lidar.

Due to space restrictions in the spinner of different turbines a small size of the lidar is desirable. Following the definition of optical and electronic components a sensor concept was developed which includes the laser and transmission optics, an industrial PC, and all electronic modules in a single casing, Figures 2 and 3. The casing is gas proof and filled with inert gas, and made of alu-

minium protected with chromate coating to prevent a loss of electrical conductivity due to oxidation and resultant degradation of electromagnetic compatibility. The four side surfaces carry heat sinks for passive cooling of electronic components, Figure 4; fans are not used because of their poor reliability.
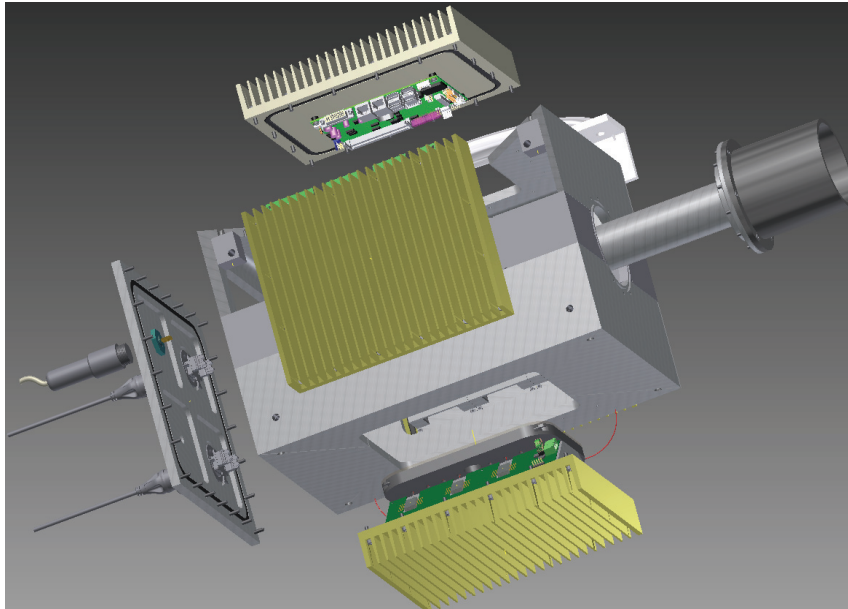

Figure 4: Exploded view, with the back plate carrying plugs for electric power and Ethernet communication, heat sinks for electronic modules, and mechanical holders of the detection optics.

Another requirement is the eye-safe operation of the instrument according to IEC 60825 by choosing an appropriate laser, preferably a Class 1M type which is safe unless focussing optics are used to narrow the beam. With a pulsed laser, the most suitable spectral range is the near infrared at 1,510-1,560 nm where, following IEC 60825, the maximum permissible energy density is 1 J/cm^2 with pulsed laser beams having pulse lengths between 1 ns and 1 μs.

Small size and passive cooling of the lidar have consequences on the selection of a laser with should have a small size and low power consumption, and therefore also a limited optical output power. Another criterion is the coherence of laser radiation. Two methods of measuring the Doppler shift with lidar are in use (5,6):

➢ the direct (incoherent) method, where the frequency shift of the returned signal is directly compared with the emitted frequency

➢ the coherent (heterodyne) method, where the returned signal is mixed with the emitted signal, yielding their frequency deviation – i.e., the Doppler shift Δf_D in Eq. (1) – as the intermediate frequency.

While the direct detection requires a laser emitting sufficiently monochromatic radiation of not much more than some Megahertz bandwidth, a lower frequency bandwidth and noise and higher frequency stability are necessary for the coherent method. On the other hand, heterodyne mixing of the local and the returned laser frequencies makes the method insensitive to ambient daylight radiation, whereby the ambient light must be precisely measured to an accuracy of 1-2 % with a direct lidar (5). Environmental changes such as temperature variations do not affect the operation of a coherent lidar. Moreover, heterodyne detection has a potential sensitivity down to single photon detection. It is limited by the shot noise of the local oscillator only (6,21), and therefore receiving optics with large aperture are not necessary. For these reasons the coherent detection method has been chosen for *Whirlwind 1*.

Laser and signal detection

In a coherent lidar, the laser consists of the following elements:

> ➢ a continuous wave (CW) laser emitting radiation having a single frequency with high stability. Its output is the local reference signal for heterodyne mixing with the Doppler-shifted backscattered radiation, and the seeding radiation of a laser amplifier (seed laser)
> ➢ a laser amplifier which converts a fraction of the CW laser radiation into high power pulses emitted to the atmosphere. The pulse length τ determines the range resolution Δr of the lidar, Figure 1, according to Eq. (2).

Three types of lasers have been used in coherent wind lidars: CO_2 lasers (e.g., 22) and solid state lasers (e.g., 23) with high output power for long-range applications, and fibre lasers (e.g., 24). Preliminary investigations were performed with fibre laser prototypes (25) and a specific configuration was selected for Doppler wind measurements. The availability of efficient fibre-based components (26) allows for an all-fibre optical configuration with *Whirlwind 1*.

The laser and detector setup is depicted in Figure 5. A Redfern Integrated Optics, Inc. RIO ORION[TM] CW single-mode laser diode (SF Laser) emits a stable single-frequency radiation with 3 kHz bandwidth at 1,550.12 nm wavelength (ITU channel 34) (27). Its 20 mW output power is divided with a beam splitter into the local reference signal illuminating two detectors, and a fraction which is fed by circulator C1 to an acousto-optical modulator (AOM) and a Bragg reflection grating (G1). The grating reflects ≈98% of the radiation passing the AOM a second time. The AOM is used to cut out pulses with a $\tau \approx 200$ ns FWHM pulse length at 10 kHz repetition rate.
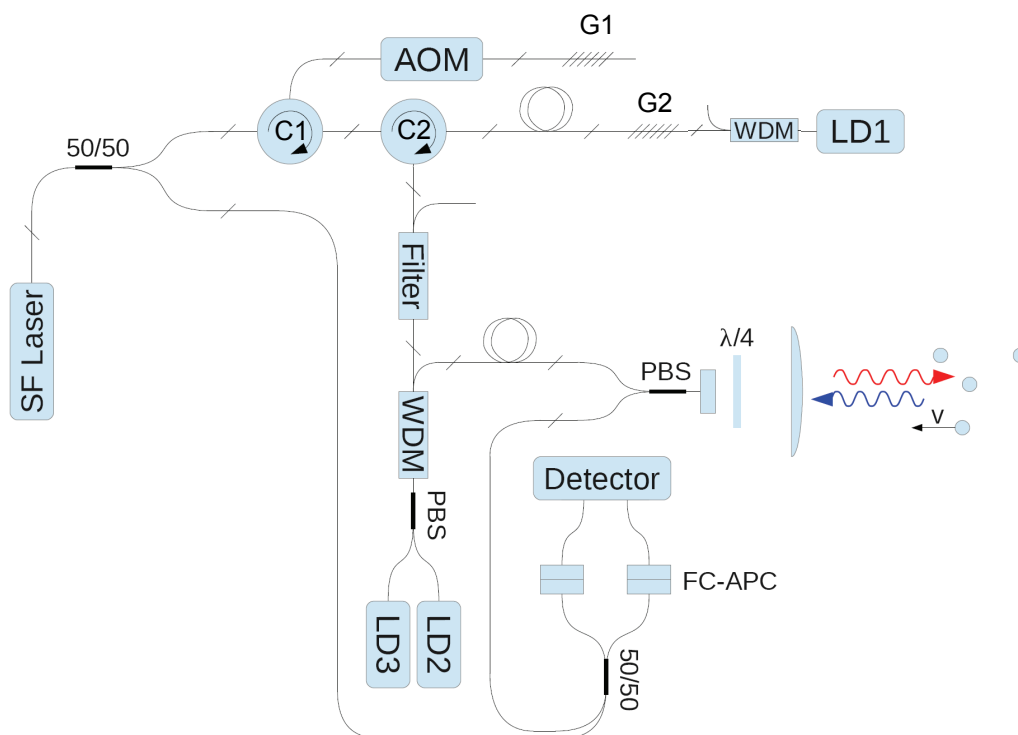

Figure 5: Schema of the laser and detector setup, explanations are given in the text. Abbreviations: 50/50: beam splitter. SF Laser: Single frequency laser. C1-2: circulators. LD1-3: laser diodes. G1-2: Bragg gratings. WDM1-2: wavelength division multiplexers. PBS: polarising beam splitter. λ/4: quarter wave retarder. FC-APC: Fibre Channel - Angled Physical Contact, a polarisation preserving fibre connector.

The electronic lidar signal processing described below yields values of the Doppler frequency shift Δf_D which is positive or negative depending on the wind direction, but its sign cannot be determined. To avoid this ambiguity of the measured wind direction the pulsed radiation frequency is shifted by f_{shift} to higher frequencies such that heterodyne mixing of Doppler shifted backscatter and local reference yields an intermediate frequency f_{IF} which is positive for all relevant line-of-

sight wind speeds,

$$f_{IF} = f_{shift} \pm \Delta f_D > 0 \qquad (3)$$

The frequency shift f_{shift} is done with the AOM. Modulated with 70 MHz the double passed AOM downshifts the radiation frequency by $f_{shift} = 140\,\text{MHz}$. Because of the minimum time bandwidth product of $\Delta f \cdot \tau \approx 0.4$ the laser pulse bandwidth increases to about 2 MHz.

The pulses are fed via C1 and C2 to a double pass pre-amplifier stage consisting of an active Er^+-doped fibre pumped by a fibre-coupled laser diode (LD1) with a max. 560 mW output power at 978 nm. Grating G2 reflects the amplified 1,550 nm laser pulses back to C2. A wavelength division multiplexer (WDM 1) with high reflectance at 1,550 nm protects LD1 from the 1-2% radiation intensity passing the grating which might otherwise destroy the diode. The WDM is transparent for the 978 nm radiation from LD1.

The pre-amplified pulses are fed *via* C2 to an optical filter which transmits the 1,550 nm laser radiation and absorbs radiation at other wavelengths which originates from amplified spontaneous emission (ASE) in the pre-amplifier. They are further amplified in the main amplifier stage which consists of an active Er^{3+}/Yb^{3+}-doped fibre pumped by two laser diodes LD2 and LD3 with characteristics identical to those of LD1. A WDM again protects the laser diodes while its 'common out' fibre deflects the pre-amplified 1,550 nm laser pulses to the active fibre. The output of LD1-3 is chosen to be less than about 400 mW, since a higher power results in stimulated Brillouin scattering (SBS) in the active fibres (28). SBS reduces the laser pulse peak power and cannot be blocked by the gratings and wavelength division multiplexers with the risk of destroying the laser diodes.

The amplified radiation is coupled out of the fibre with a polarisation preserving fibre connector. It passes a quarter-wave retarder for conversion of linear to circular polarisation. A diffraction-limited optical lens is used to shape a laser beam with 4 cm diameter and a 25 µrad beam divergence half angle. This small beam divergence results in a size of the sounding volume which is increased by not more than 1% over a measuring range of 500 m. The average optical power is 100…150 mW, the pulse length is 200 ns FWHM and the repetition rate is 10 kHz.

Backscattering from aerosols is collected by the same lens. Its circular polarisation is converted to linear polarisation with an orientation which is perpendicular to the linear polarisation of the laser radiation. A polarising beam splitter (PBS) deflects the backscattered radiation to a 50/50 beam splitter, where it is added to the local reference from the SF laser. The two beam splitter output fibres illuminate two photodiodes. Their photocurrents are subtracted, whereby the signal background from ambient light cancels out. The residual signal is the intermediate frequency f_{IF} superimposed by electronic shot noise.

The 120 dB amplified photodiode signal is digitized to 8 bit with a 400 MHz sampling rate. A Fast Fourier Transform converts the signal to a discrete spectrum at 128 discrete frequencies from which 64 frequency contributions to the signal in steps of 3.125 MHz can be retrieved. In Eq. (3), still air corresponds to $\Delta f_D = 0$ and $f_{IF} = f_{shift} = 140\,\text{MHz}$. A line-of-sight wind speed against and with the laser beam direction decreases and increases f_{IF}, respectively. Considering the application to be a wind sensor in the spinner of a wind turbine the measuring range of wind speeds should be asymmetric. It is set to -20 to +100 m/s for wind with and against the laser beam direction. There are 37 range gates, each 30 m long, and a 50% overlapping is applied.

Electronics

The lidar is equipped with an industrial single board iBASE IB905 personal computer with a Windows 7 operating system, mounted on a heat sink which is attached at the side of the lidar casing. The lidar instrument control is realised with LabVIEW® as a visual programming language. Remote communication with the lidar and data read-out is done via TCP-IP. In case of a missing communication sensor data including all raw data can be stored for a measuring period of 140 days.

Fast processes like, e.g., analogue-to-digital conversion of the photodetector signals and their Discrete Fourier Transformation (29) make a Field Programmable Gate Array (FPGA) module necessary. A Spartan 6 LX-150 FPGA was chosen and implemented on an electronic board which in-

cludes the photodetectors, the photo-amplifiers, the Analogue-to-Digital-Converter, and other electronic sub-components, Figure 6. Critical elements with respect to temperature are placed on the soldering side of the printed circuit board and are flange mounted on the main board heat sink to transport the dissipated power out of the casing. All components are specified for an operating temperature range of -40 to +55°C.
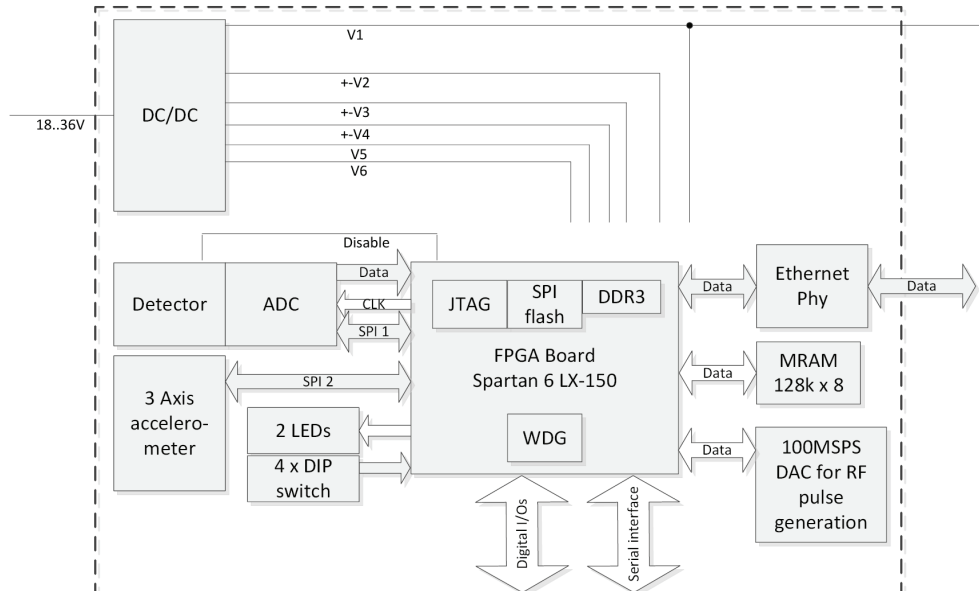

Figure 6: Circuit board schematics with signal detection, Field Programmable Gate Array, pulse generator for modulating the AOM, a three-axis accelerometer for detecting the instrument orientation, and other electronic components. JTAG: Joint test action group, an interface for FPGA programming; SPI flash: Serial Peripheral Interface Bus flash memory for FPGA programme storage MRAM: Non-volatile memory for changeable instrument parameters.

RESULTS

Data processing

The emitted laser beam interacts with aerosols and this leads to a change of the frequency of the radiation scattered by these particles in the presence of wind through the Doppler effect. The time-resolved signal return is divided to a series of range gates and, after conversion, to a frequency spectrum. The frequency peak for each range gate is determined using a parabolic curve fit. The frequency peak is the information from which the wind velocity is calculated using Eq. (1).

To qualitatively decide, whether the determination of the frequency peak is accurate enough, a computer simulation was programmed, where an output frequency peak is compared with an input signal frequency, that has been subjected to a simulated noise signal, then processed in the same way as the lidar backscattered signal. The steps of the signal simulation are shown in Figure 7.

The simulation starts by introducing a sine wave of frequency f_{in}. The input frequency is set to be variable, so that a precise observation of the behaviour of the simulated signal under different conditions could be perceived. In a first step, artificial noise signals with different colours (e.g. pink or blue background noise) were added to the sine wave to test the behaviour of different noise reduction methods and the accuracy of the peak detection using different colours of noise. Later on, a real background signal of the lidar was added to the input sine wave signal as a noise source in the simulation. A Fast Fourier Transform (FFT) converts the time domain signal to a discrete spectrum at 128 discrete frequencies. The spectra for the same range gate from successive pulses are then averaged over 1,000 pulses to increase the Signal-to-Noise Ratio (*SNR*) and therefore improve the detection sensitivity. After averaging the spectra, different noise reduction (also called denoising) methods, for example noise whitening, were investigated. After denoising the signal, the frequency peak is determined for each range gate using a parabolic curve fit.
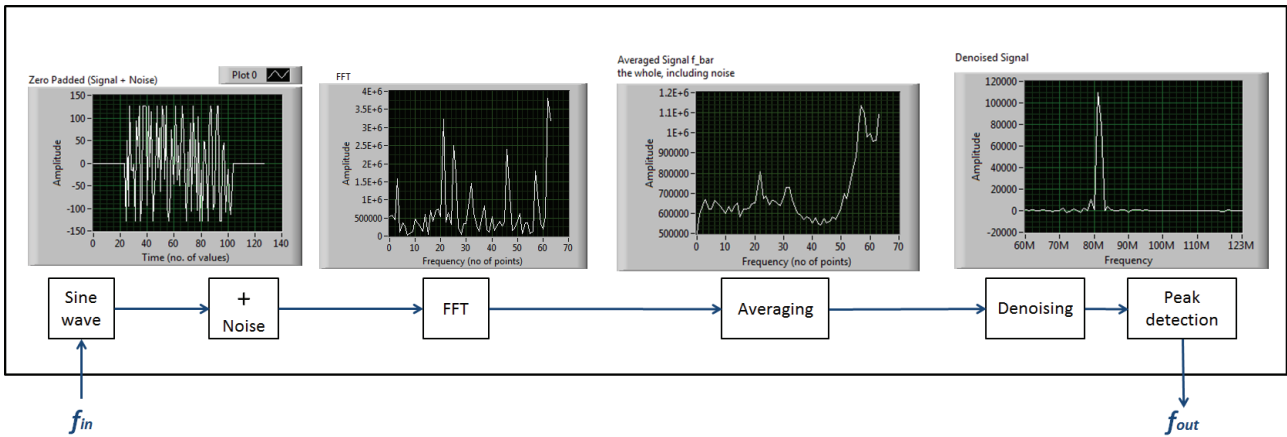
Figure 7: Steps of the lidar signal simulation on Labview®. f_{in}: Input frequency, f_{out}: output frequency. Peak detection method: Parabolic fit.

After deriving the peak frequency f_{out} for each of the input frequencies, relationships between f_{in} and f_{out} as well as for f_{in} and $f_{out} - f_{in}$ are represented in graphs, Figure 8. Optimally, the graphical relationship between f_{in} and f_{out} is a straight line, hence, $f_{out} = f_{in}$. The mean square error (*MSE*) is used to quantify the difference between frequency values implied by an estimator (f_{out} values) and the true frequency f_{in}. The *MSE* is then calculated using Eq. (4):

$$MSE = \frac{1}{n}\sum_{i=1}^{n}\left(\hat{Y}_i - Y_i\right),\qquad(4)$$

where $\hat{Y}$ is a vector of n predictions, and Y is the vector of the true values.

The behaviour of simulated signals, i.e., the relationship between f_{in} and f_{out}, differs when introducing different colours of background noise. The difference can be noticed when comparing the resulting mean values. It was also found that the frequency estimation error has a periodic characteristic (Figure 8). When the input frequency lies between two discrete steps, the output frequency $\underline{f_{out}}$ equals the input frequency f_{in}. At a higher input frequency, one obtains a lower output frequency, and at a lower input frequency (on the left-hand side of a discrete step) the output frequency is higher.
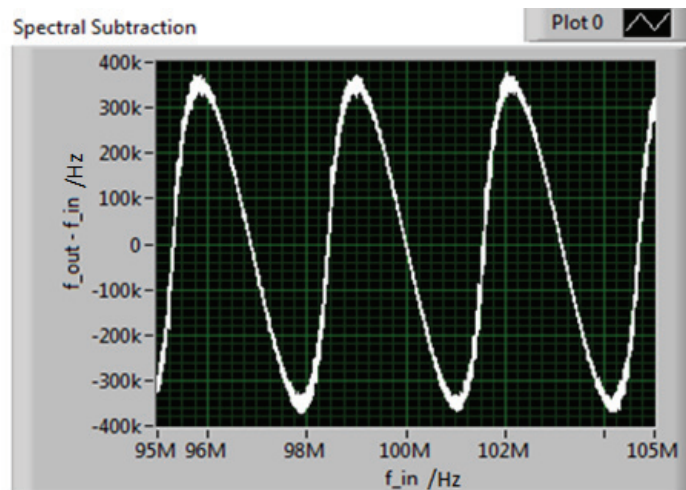

Figure 8: Graphical representation of the frequency estimation error. X-axis: fin, Y-axis: fout-fin. Frequency range: from 95 MHz to 105 MHz in 1 kHz steps (high resolution). Denoising method: Spectral Subtraction

A more detailed analysis of signal processing methods and a description of procedures allowing these frequency estimation errors to be significantly reduced shall be reported in a separate publication.

Wind data

Test measurements were performed in the laboratory through the window with the lidar oriented at an inclined angle, measuring wind speeds along the line-of-sight. Figure 9 shows an example of the results obtained during these tests. In the upper graph, a gust can be identified which is approaching with a line-of sight wind speed of approx. 6 m/s at 450 m decreasing to 3 m/s at 150 m distance. Data of the first 30 m are not valid due to the trailing edge of the outgoing laser pulse which interferes with the backscatter signal at this close distance and degrades the signal. The time series of wind speed at selected distances shown in the lower graph further depicts the turbulence characteristics of the gust.
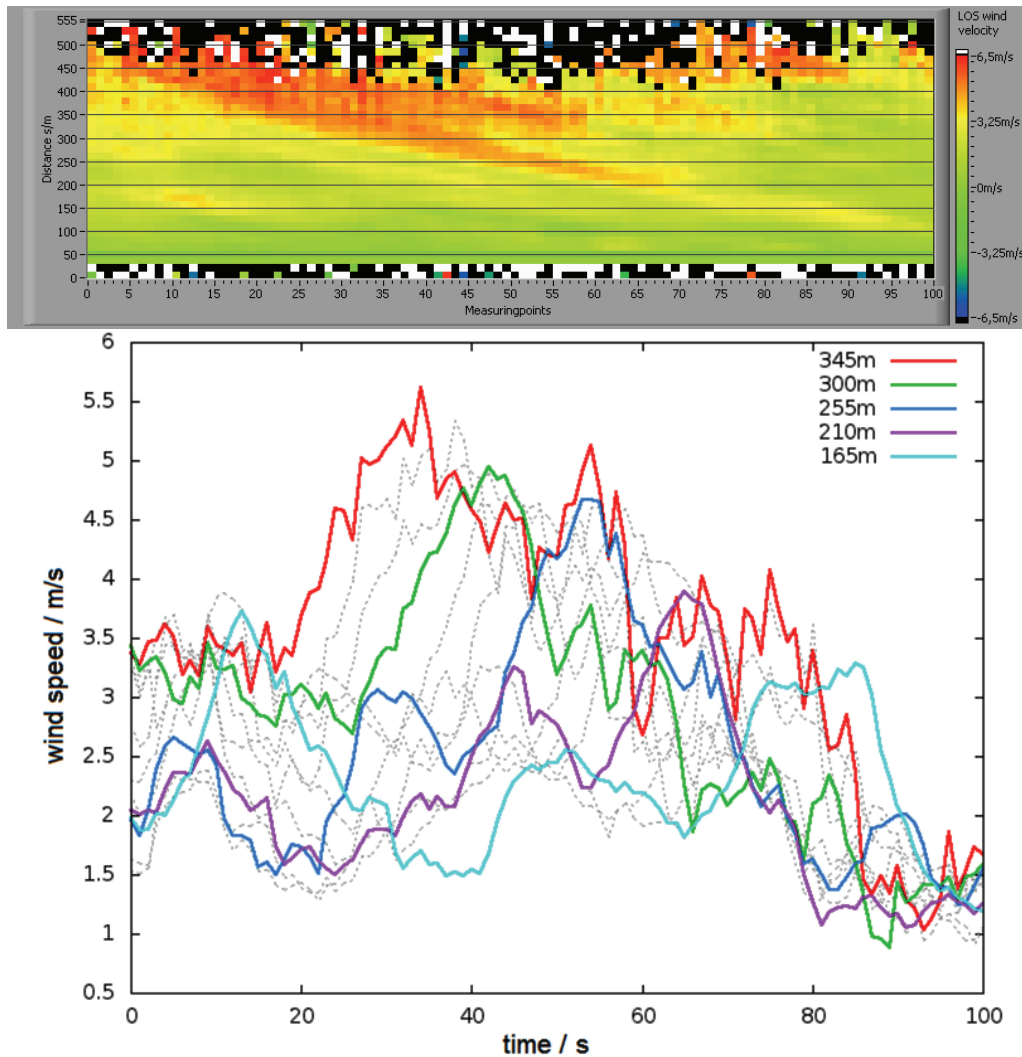

Figure 9: above: Wind speed measured in a laboratory test through the window on 10 July 2014 at a zenith angle of approx. 60°. Measuring points correspond to the time in seconds. 10,000 single pulse data were averaged which corresponds to a 1 s averaging. Below: Wind speeds at selected distances from the same measurement. Thin dotted lines correspond to distances at 15 m intervals between the coloured lines.

On 17 July 2014 *Whirlwind 1* was installed on a wind turbine at position 54°00'N 06°35'E in the Research at Alpha Ventus (Rave) offshore test field, German Bight. In a first approach, the instrument has been mounted in a metallic frame on top of the nacelle, instead of integrating the instrument into the spinner, Figure 10. A scanning operation is not possible in this configuration. Above *Whirlwind 1* a Leosphere WINDCUBE® lidar is mounted which allows comparative measurements of the incoming wind to be performed. These tests are in progress, and results will be reported in the near future.

Figure 10: Lidar installation on the nacelle of a wind turbine in the RAVE offshore test field. Mounted on top of the frame is a Leosphere WINDCUBE® lidar combined with the Stuttgart Wind Energy (SWE) Scanner from DEWI GmbH, Wilhelmshaven. Whirlwind 1 is mounted in the inner frame structure on the right. Photo courtesy: Jan Anger, University of Stuttgart, Germany.

First wind measurements obtained at this location are shown in Figure 11. The screenshot depicts part of the sensor and data control windows and functionalities available with LabVIEW®. In this example, the shortest signal integration time has been chosen to visualise the shading of the path of rays by turning rotor blades. Due to this and because of clear atmospheric conditions and low backscatter intensities the detection range is not more than 150 m. However, the instrument still works within the expected specifications under these conditions.
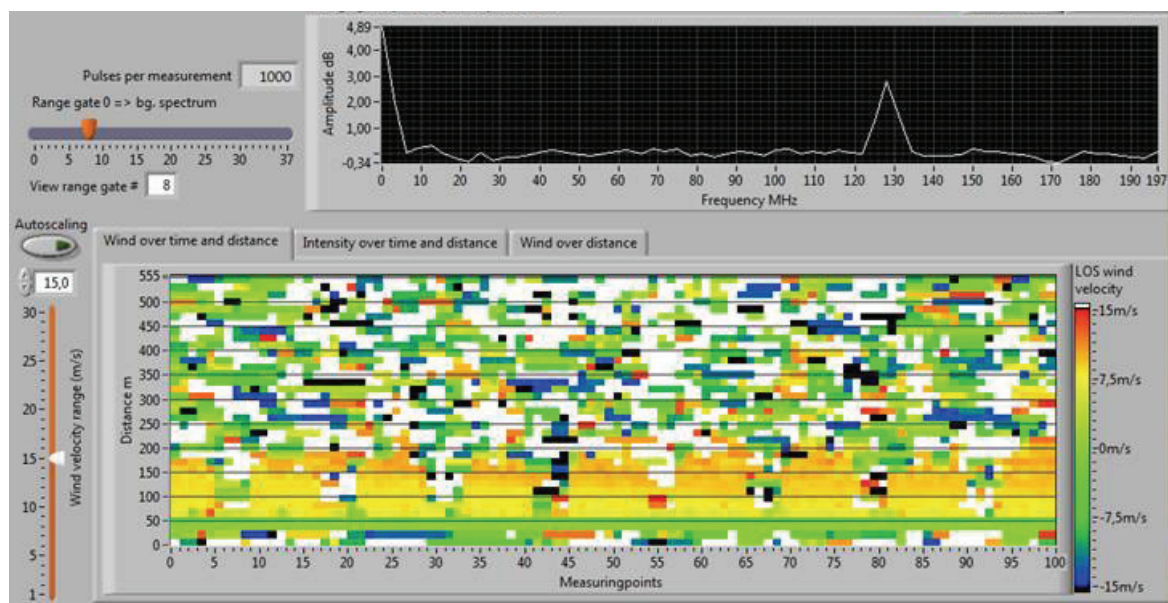

Figure 11: Measurements taken on 20 August 2014. Upper panel: FFT spectrum of the returned backscatter in range gate 8 corresponding to a distance of 105 – 135 m. The peak at 128 MHz corresponds to a wind speed of 9.3 m/s. Lower panel: Averaging over 1,000 pulses or 0.1 s and low aerosol concentrations reduce the detection range to 150 - 200 m. Every 0.7 s the airfoils prohibit measurements for about 0.4 s.

DISCUSSION AND CONCLUSIONS

Whirlwind 1 is a compact and robust Doppler wind lidar developed for use in harsh environmental conditions. Following successful tests in laboratory conditions first applications in an offshore wind farm have demonstrated its performance to measure wind data when exposed to free-air weather conditions. In a next step, the formal specifications shall be further evaluated through approved test laboratories, covering both

> ➤ the environmental performance in terms of vibration, temperature, electromagnetic noise etc., as well as

> ➤ the precision of measured wind speeds by comparison with mast data from calibrated anemometers.

While the instrument is capable of detecting wind in the range of -20 to +100 m/s, the resolution of wind speed data is not yet fully satisfying. Based on the 400 MHz sampling rate of the 8 bit digitiser the sensor detects wind speed at discrete 2.4 m/s intervals. Processing of the Fourier spectra mentioned allows for a more accurate identification of the Doppler shifted peak so that the maximum error of wind speed is less than 0.5 m/s. Further improvements are presently investigated and it is expected that a resolution of about 0.1 m/s will be achieved. The results will be reported in the near future. This will enable us to perform improved analyses of statistical parameters of turbulence characteristics (30) and, in particular, to improve the filtering effect due to the size of the sounding volume (20). In contrast to CW Doppler lidars and due to the very small 25 µrad divergence half angle of the laser beam, the sounding volume remains virtually unchanged over the entire measuring range which will make *Whirlwind 1* a very suitable instrument for these studies.

Besides spinner-based upwind measurements where the instrument is scanning due to the turning rotor, an application for downstream measurements of wind turbine wake dynamics may be achieved as well, if a nacelle-mounted version is combined with an optical scanner. Technical solutions shall be investigated in the near future.

Besides these turbine-mounted remote wind measurements for an improved control of turbine operations, other applications may include a ground-based assessment of wind resource in the context of wind farm planning. For this, a vertical profiling of wind velocities can be achieved with a pillar mounted version using an antenna rotor, Figure 12. It enables profiles of horizontal wind velocities to be measured up to approx. 400 m above ground. This version presents a most compact, easy-to-use ground-based pulsed Doppler lidar available for all-weather operations, whereby its low weight and small size makes it suitable also in complex terrain.
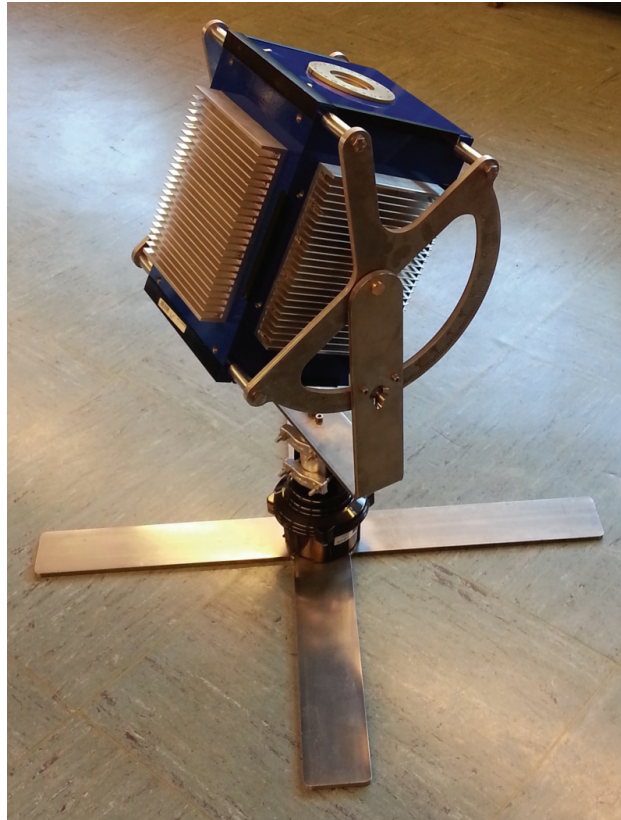
ACKNOWLEDGEMENTS

Figure 12: Demonstration model of a ground-based Doppler lidar using Whirlwind 1 for measuring vertical profiles of wind velocity.

REFERENCES

1   Antoniou I & H E Jørgensen (Editors), F Ormel, S Bradley, S von Hünerbein, S Emeis & G Warmbier, 2003. On the Theory of SODAR Measurement Techniques. Final reporting on WP1, EU WISE Project NNE5-2001-297, Report No. Risø-R-1410(EN) (Risø National Laboratory, Roskilde, Denmark) April 2003, 60 pp

2   Measures R M, 1984. Laser Remote Sensing. Fundamentals and Applications (Wiley, New York) 510 pp.

3   Weitkamp C (Editor), 2005. Lidar. Range-Resolved Optical Remote Sensing of the Atmosphere. Springer Series in Optical Sciences, Vol. 102 (Springer: Berlin, Heidelberg, New York) 456 pp.

4   Fujii T & T Fukushi, 2005. Laser Remote Sensing (Taylor & Francis, Boca Raton) 888 pp.

5   Werner C, 2005. Doppler Wind Lidar. In: Lidar. Range-Resolved Optical Remote Sensing of the Atmosphere, edited by C Weitkamp. Springer Series in Optical Sciences, Vol. 102 (Springer: Berlin, Heidelberg, New York) 325-354

6   Henderson S W, P Gatt, D Rees & R M Huffaker, 2005. Wind Lidar. In: Laser Remote Sensing, Chapter 7, edited by T Fujii & T Fukushi (Taylor & Francis, Boca Raton) 469-722

7   Brown A, E L Thomas, R Foord & J M Vaughan, 1978. Measurements on a distant smoke plume with a CO_2 laser velocimeter. Journal of Physics D: Applied Physics, 11(2), 137-145

8   Albers A, A W Janssen & J Mander, 2008. Comparison of lidars, German Test Station for remote wind sensing devices. 9th German Wind Energy Conference DEWEK 2008, 4 pp. (last date accessed: 15 Sept 2014)

9   Käsler Y, S Rahm, R Simmet & M Kühn, 2010. Wake measurement of a multi-MW wind tur-
     bine with coherent long range pulsed Doppler wind lidar. Journal of Atmospheric and Oceanic
     Technology, 27, 1529-1533

10   Courtney M, R Wagner & P Lindelöw, 2008. Testing and comparison of lidars for profile and
     turbulence measurements in wind energy. IOP Conference Series, Earth and Environmental
     Science, 1(1), 012021, 14 pp.

11   Westerhellweg A, B Canadillas, A Beeken & T Neumann, 2010. One year of lidar measure-
     ments at FINO1-Platform: Comparison and verification to met-mast data. 10th German Wind
     Energy Conference DEWEK 2010, 5 pp. (last date accessed: 15 Sept 2014)

12   Lang S & e McKeogh, 2011. LIDAR and SODAR measurements of wind speed and direction
     in upland terrain for wind energy purposes. Remote Sensing, 3(9), 1871-1901

13   Görner K, A Westerhellweg & S Brillet, 2010. Seasonal correction of short-term sodar and lidar
     measurements for use in energy yield assessments of wind farms. 10th German Wind Energy
     Conference DEWEK 2010, 4 pp. (last date accessed: 15 Sept 2014)

14   Bradley S, 2008. Wind speed errors for LIDARs and SODARs in complex terrain. IOP Confer-
     ence Series, Earth and Environmental Science, 1(1), 012061, 7 pp.

15   Magee E P, T J Kane & R G Frehlich, 1998. Bistatic coherent laser radar performance. Geo-
     science and Remote Sensing Symposium Proceedings, 1998. IGARSS '98, Vol. 5, 2433-2435

16   Bradley S, S von Hünerbein & T Mikkelsen, 2012. A bistatic sodar for precision wind profiling
     in complex terrain. Journal of Atmospheric and Oceanic Technology, 29, 1052-1061

17   Trujillo J J, F Bingöl, G C Larsen, J Mann & M Kühn, 2010. Light detection and ranging meas-
     urements of wake dynamics. Part II: two-dimensional scanning. Wind Energy, 14, 61-75

18   Schlipf D, D J Schlipf & M Kühn, 2012. Non-linear model predictive control of wind turbines
     using LIDAR. Wind Energy, doi: 10.1002/we.1533, 23 pp.

19   Wagner R, T F Pedersen, M Courtney, I Antoniou, S Davoust & R L Rivera, 2013. Power
     curve measurement with a nacelle mounted lidar. Wind Energy, doi: 10.1002/we.1643, 13 pp.

20   Mikkelsen T, N Angelou, K Hansen, M Sjöholm, M Harris, C Slinger, P Hadley, R Scullion, G
     Ellis & G Vives, 2013. A spinner-integrated wind lidar for enhanced wind turbine control. Wind
     Energy, 16(4), 625-643

21   Yariv A, 1991. Optical Electronics, 4th Edition (Oxford University Press, USA) 736 pp., 407-11

22   Werner C, P H Flamant, O Reitebuch, F Köpp, J Streicher, S Rahm, E Nagel, M Klier, H
     Herrmann, C Loth, P Delville, P Drobinski, B Romand, C Boitel, D Oh, M Lopez, M Meisson-
     nier, D Brunneau & A Dabas, 2001. Wind infrared Doppler lidar instrument. Optical Engineer-
     ing, 40(1), 115-125

23   Henderson S W, P J M Suni, C P Hale, S M Hannon, J r Magee, D L Bruns & E H Yuen, 1993.
     Coherent laser radar at 2 µm using solid-state lasers. IEEE Transactions on Geoscience and
     Remote Sensing, 31(1), 4,15

24   Kameyama S, T Ando, K Asaka, A Hirano & S Wadaka, 2007. Compact all-fiber pulsed coher-
     ent Doppler lidar system for wind sensing. Applied Optics, 46(11), 1953-1962

25   Beier F, O de Vries, T Schreiber, R Eberhardt, A Tünnermann, C Bollig, P G Hofmeister, J
     Schmidt & R Reuter, 2013. Robust 1550-nm single-frequency all-fiber ns-pulsed fiber amplifier
     for wind-turbine predictive control by wind lidar. In: SPIE Proceedings Vol. 8601, Fiber Lasers
     X: Technology, Systems, and Applications, edited by S Hendow. DOI: 10.1117/12.2004244 , 7
     pp.

26 Hobbs P C D, 2009. Building Electro-Optical Systems. Making it All Work. Chapter 8: Fiber Optics, pp. 262-308 (Wiley, Hoboken, New Jersey) 799 pp.

27 International Telecommunication Union (ITU), 1999. G.692: Optical interfaces for multichannel systems with optical amplifiers, Article Number E 14418 (last date accessed: 15 Sept 2013)

28 Agrawal G P, 2006. Nonlinear Fiber Optics. 4th Edition. Chapter 9: Stimulated Brillouin Scattering, pp. 329-376 (Academic Press) 529 pp.

29 Diniz P S R, E A B da Silva & S L Netto, 2010, Digital Signal Processing: System Analysis and Design. Second Edition (Cambridge University Press) 889 pp.

30 Frehlich R, 1997. Effects of wind turbulence on coherent Doppler lidar performance. Journal of Atmospheric and Oceanic Technology, 14, 54-75